Journal of Power Sources 195 (2010) 6817–6824

Contents lists available at ScienceDirect

Journal of Power Sources

journal homepage: www.elsevier.com/locate/jpowsour

Characterizing capacity loss of lithium oxygen batteries by impedance spectroscopy

Mojtaba Mirzaeian*, Peter J. Hall[1]

Department of Chemical and Process Engineering, University of Strathclyde, Glasgow G1 1XJ, Scotland, UK

ARTICLE INFO

Article history:
Received 12 January 2010
Received in revised form 3 March 2010
Accepted 20 April 2010
Available online 27 April 2010

Keywords:
Lithium oxygen battery
Carbon aerogel
Charge–discharge cycling
Discharge capacity
Electrochemical impedance spectroscopy

ABSTRACT

Polymer based carbon aerogels were prepared by synthesis of a resorcinol formaldehyde gel followed by pyrolysis at 1073 K under Ar and activation of the resultant carbon under CO_2 at different temperatures. The prepared carbon aerogels were used as active materials in the preparation of cathode electrodes for lithium oxygen cells and the electrochemical performance of the cells was evaluated by galvanostatic charge/discharge cycling and electrochemical impedance measurements. It was shown that the storage capacity and discharge voltage of a Li/O_2 cell strongly depend on the porous structure of the carbon used in cathode. EIS results also showed that the shape and value of the resistance in the impedance spectrum of a Li/O_2 cell are strongly affected by the porosity of carbon used in the cathode. Porosity changes due to the build up of discharge products hinder the oxygen and lithium ion transfer into the electrode, resulting in a gradual increase in the cell impedance with cycling. The discharge capacity and cycle life of the battery decrease significantly as its internal resistance increases with charge/discharge cycling.

1. Introduction

There is currently considerable interest in the use of renewable energy sources as clean and efficient energy supplies because of serious concerns about the anticipated doubling of world energy consumption within the next 50 years [1], and also due to intense interest in the use of low – or even zero – emission energy sources as the world strive to reduce greenhouse gas emissions. Energy in the form of electricity generated from renewable energy sources, such as solar, wind and tidal, offers enormous potential for powering our future energy demands. The use of these intermittent energy sources to meet our continuous energy needs is only possible when efficient storage technologies with higher energy and power densities, and capable of storing and delivering energy with longer calendar and cycle lifetimes are developed.

Batteries, as chemical energy storage devices, are at the forefront of electrical energy storage systems by storing energy in the form of chemical reactants capable of generating charge. These electrical energy storage systems have been available for many decades; however the introduction of rechargeable lithium ion batteries in the 1990s for powering the portable electronics was a revolutionary breakthrough in battery technology to swing away from the previous low voltage aqueous systems such as lead acid, Ni–Cd and NiMH batteries [2]. Non-aqueous lithium batteries employ a wide range of electrode and electrolyte materials and use a various number of electrochemical couples [3–9] to enhance the storage capacity and improve the safety of energy storage systems but the most common anode and cathode materials in current lithium ion cells are graphite and lithium cobalt oxide respectively [10]. Although with this configuration the safety of lithium batteries is improved as lithium is contained within a host structure both at the anode and the cathode, but the battery capacity is limited mainly by the positive electrode and does not exceed 140 mAh g^{-1} [11]. Several alternative approaches are considered to enhance the storage capacity of lithium ion batteries but these methods will increase the energy density of the cathode only by a factor of 2 which is not enough to power our modern lifestyles demand [10,12].

Metal/air batteries have a much higher specific energy than most available primary and rechargeable batteries which is critical for applications that are very sensitive to weight. Among different metal/air couples such as Zn/air, Al/air, and Mg/air [13–18], the Li/air couple using a non-aqueous electrolyte is especially attractive as it couples Li, the less electronegative material, with oxygen through a catalyzed air electrode and it is unique in that, molecular oxygen as cathode active material is absorbed from air and is not stored in the battery. This system has a theoretical specific energy of 13 kWh kg^{-1} assuming a cell voltage of 3.4 V [19], though only 2.85 V is achieved in practice. A non-aqueous electrolyte lithium oxygen battery was first introduced by Abraham and Jiang in 1996 [20]. The cell was shown to have an operating voltage of 2.0–2.8 V,

* Corresponding author. Tel.: +44 141 548 2075; fax: +44 141 552 2539.
E-mail addresses: mojtaba.mirzaeian@strath.ac.uk (M. Mirzaeian), p.j.hall@strath.ac.uk (P.J. Hall).
[1] Tel.: +44 141 548 4084; fax: +44 141 552 2539.

0378-7753/$ – see front matter © 2010 Elsevier B.V. All rights reserved.
doi:10.1016/j.jpowsour.2010.04.064

with a catalytic air electrode recharging over several cycles. The discharge mechanism was determined to be primarily the deposition of Li_2O_2 in a carbon-based air electrode. The battery has the potential to dramatically increase the storage capacity and energy density of current lithium batteries and overcome the corrosion and safety concerns of the past plagued lithium air systems, but its cyclability is limited as the end-of-discharge is reached when insoluble discharge products, Li_2O and Li_2O_2, fill pores of the air cathode electrode [21]. Despite several studies such as: the effects of air electrode formulation and electrolyte composition [22]; mechanism of charge/discharge catalytic reaction and role of catalyst [12]; and optimization of electrode porous structure [23], on the performance of organic electrolyte lithium oxygen batteries, yet much is to be done to understand the performance limitations of this system from safety and charge discharge cycling viewpoints and also the processes that govern the battery's operation.

In the present study, resorcinol formaldehyde carbon aerogels with controlled porous structure were synthesized and their performance as active material in the air electrode of a lithium oxygen battery was evaluated. Electrochemical impedance spectroscopy (EIS) has been applied to study the interfacial changes occurring at the cathode electrode prepared from the aforementioned carbon aerogels with different porous structure, and to understand the cell capacity loss with charge/discharge cycling.

2. Experimental

Preparation of carbon aerogels and their organic precursors has been described elsewhere [24]. Resorcinol and formaldehyde both from Aldrich were mixed in 1:2 molar ratio with adding appropriate amount of water and sodium carbonate as polymerization catalyst. After stirring to form a homogeneous solution, the mixture was poured into a glass vial, sealed and cured at an elevated temperature. The gel for this study was synthesized at a [Resorcinol]/[Catalyst] (R/C) ratio of 600. Upon the completion of the curing process, the hydrogel was solvent exchanged by immersing in acetone to ensure complete replacement of the water that previously occupied the pores of the gel. Acetone exchanged resorcinol–formaldehyde (RF) aerogel was then filtered and dried at 353 K under vacuum for 3 days. The RF aerogel was subsequently carbonized in a tubular furnace under Ar at 1073 K. Activated carbon aerogels were prepared by activation of the resultant carbon aerogel in a tubular furnace under CO_2 at different temperatures and times.

The porosity of RF aerogel and carbon aerogels were studied by the analysis of nitrogen adsorption–desorption isotherms measured by an ASAP 2420 adsorption analyzer (Micromeritics) at 77 K. The samples were evacuated at 373 K for 2 h prior to the adsorption measurements. BET method was used for surface area measurements, BJH adsorptions–desorption was used for mesopore analysis and t-plot method was used for micropore analysis. Total pore volume was calculated from the adsorbed volume of nitrogen at $P/P_0 = 0.99$ (saturation pressure). Pore size distributions were obtained by the BJH method from adsorption branch of the isotherms [25].

Cathode oxygen electrodes were prepared by mixing 11 wt% milled porous carbon aerogel with 19 wt% electrolytic manganese dioxide (EMD) as catalyst, 15 wt% Kynar Flex 2801 as binder and 55 wt% propylene carbonate (PC) as wetting agent, and then casting in 200 μm thick films according to the procedure described elsewhere [21–23]. The composite electrode contains 24.5 wt% porous carbon aerogel, 42.2 wt% EMD and 33.3 wt% binder. Electrochemical cells were constructed in an argon-filled glove box, under a dry argon atmosphere with H_2O and O_2 levels less than 1.5 and 0.5 ppm respectively, using a stainless steel bar as anode current collector, a lithium metal foil as anode, a glass micro-fiber separator soaked with electrolyte (1 M $LiPF_6$ in propylene carbonate), a disc of 1.3 cm diameter cathode electrode, an aluminum mesh and a hollow aluminum bar on the top of it as cathode current collector. The cell parts were compressed together to ensure that the electrode contact is good and then the cell was completely sealed except for the Al mesh window that exposes the porous cathode to the O_2 atmosphere. The cell then was exposed to O_2, from an oxygen cylinder with a purity of 99.5%, at atmospheric pressure for a minimum of 30 min prior to the electrochemical tests and all measurements were carried out under O_2 atmosphere at 298 K.

Electrochemical performance of the prepared lithium oxygen cells were examined using a 1470E Solartron cell test system in conjunction with a 1455 frequency response analyzer. The charge and discharge cycling of the cells were conducted galvanostatically at a 70 mA g^{-1} rate in a voltage range of 2.05–4.4 V. Electrochemical impedance spectroscopy of the cells was evaluated using an AC impedance analyzer over a frequency range of 10^6 Hz to 10^{-3} Hz for interface investigation of the electrodes in cells after each charge and discharge cycle.

3. Results and discussion

N_2 adsorption–desorption isotherms at 77 K for activated carbon aerogels obtained by CO_2 activation of the RF carbon aerogel at different temperatures, are shown in Fig. 1. Activated carbons are named as AC-*x* where *x* is the activation temperature. Steep increase in the amount of gas adsorbed at low pressures is indicative of microporosity in the structure of carbons [26]. Increase in microporosity with activation temperature might be due to the creation of new micropores by oxidation of certain structural components and opening of previously inaccessible pores at higher temperatures under CO_2.

Hysteresis loops in the P/P_0 range 0.8–0.99 are indicative of mesoporosity in carbon aerogels. The lower part of the hysteresis loops represent the filling of the mesopores while the upper part represent the emptying of the mesopores [25]. For all isotherms in Fig. 1 the hysteresis loops are located almost over the same P/P_0 range showing the activation temperature does not affect the mesopore size and pore size distribution of the carbon aerogels significantly. Vertical shift in the location of hysteresis loops to higher volumes shows that the adsorption capacity increases with the activation temperature indicating the development of porosity in carbon. Porosity parameters of the carbon samples are shown in Table 1. Carbon sample activated at 1223 K shows a decrease in the

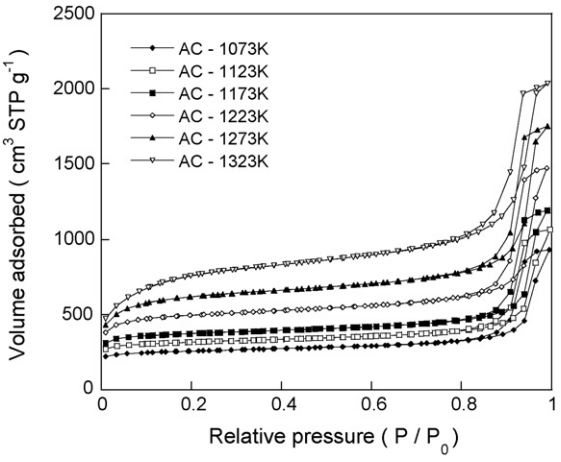

Fig. 1. Nitrogen adsorption–desorption isotherms at 77 K for carbons activated at various temperatures.

Table 1
Porosity parameters of activated carbon aerogels prepared by carbonization of a RF aerogel with R/C ratio of 600 activated under CO_2 at different temperatures.

Sample	S_{BET} ($m^2\,g^{-1}$)	V_{total} ($cm^3\,g^{-1}$)	V_{micro} ($cm^3\,g^{-1}$)	V_{meso} ($cm^3\,g^{-1}$)	$\%V_{micro}$	$\%V_{meso}$	D_{avg} (nm)
AC-1073 K	801	1.441	0.296	1.145	20	80	23.98
AC-1123 K	982	1.641	0.374	1.261	22	78	22.05
AC-1173 K	1555	2.278	0.550	1.728	24	76	20.54
AC-1223 K	1164	1.839	0.437	1.402	23	77	18.37
AC-1273 K	1674	2.375	0.502	1.873	21	79	17.80
AC-1323 K	2471	3.146	0.335	2.811	11	89	17.37

adsorption capacity probably due to the pore collapse and blockage at this temperature range [27,28]. Data given in Table 1 shows that activation at temperatures higher than 1223 K results in the opening of the blocked pores, increasing the pore volume and BET area significantly.

Fig. 2 shows that for all samples, the pore size distribution curves are centred at the same pore diameter range indicating all carbon samples are mainly mesoporous materials and possess similar pore size and pore size distribution. Fig. 2 and data given in Table 1 show that such an activation treatment results in activated carbon aerogels having high pore volumes with average pore diameters in the range of 17–24 nm.

In order to evaluate the electrochemical performance of the synthesized carbon aerogels, lithium/oxygen cells using these carbons as active material in the cathode formulation were fabricated. Open-circuit potential (OCP), discharge capacity and electrochemical impedance of the cells were measured and the capacity and impedance characteristics of the electrodes were determined. The values of OCP for fresh cells were in the range of 3.05–3.15 V.

EMD, used in the electrode formulation, aids the Li_2O_2 decomposition and charging process [21] and catalyzes the reduction of O_2 to O^{2-} on the cathode electrode during discharge process [20]. It is an intercalation host for Li and some of discharge reaction takes place on its surface [22]. Assuming that the products of the discharge reaction in Li/O_2 cell deposit only onto carbon, the discharge capacities have been normalized to the weight of carbon used in the air cathode. Taking the EMD capacity as 308 mAh g^{-1} [29], MnO_2-related capacity of the cathode electrode normalized to the weight of carbon is estimated at most 530 mAh g^{-1} as carbon and EMD contribute 24.5 wt% and 42.2 wt% to the composite cathode respectively.

In order to obtain the specific capacity of the porous carbon as active material used in the electrode formulation, this value is subtracted from the all measured cell capacities normalized to the weight of carbon used in the cathode.

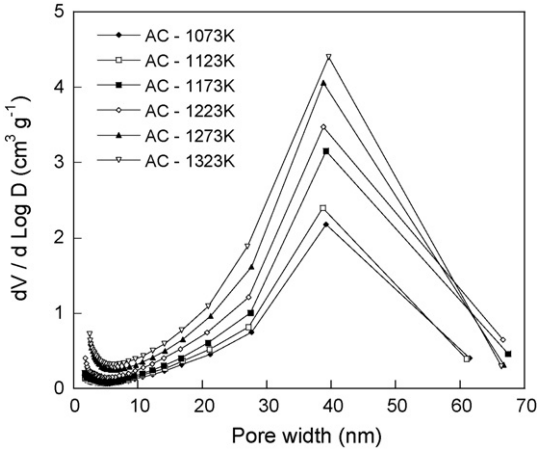

Fig. 2. Pore size distribution of carbons activated at various temperatures.

Fig. 3 shows discharge behavior of the Li/O_2 cells based on electrodes prepared from AC-*x* carbons. Variations of the cell voltage against specific capacity of composite electrodes made from porous carbon aerogels at a discharge rate of 70 mA g^{-1} show flat discharge profiles at about 2.6–2.8 V. These are associated with the storage behavior of the cells and are in good agreement with the preceding reported data for a similar cell discharged in O_2 at atmospheric pressure involving formation of Li_2O_2 [20–23]. Change in discharge voltage and discharge capacity for both composite electrodes and porous carbons with different porosity parameters are given in Table 2.

Total, micropore and mesopore volumes of activated carbon aerogels used in electrochemical measurements are shown in Fig. 4.

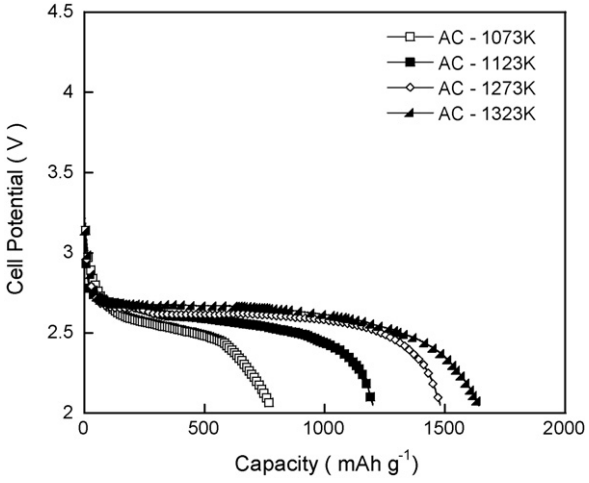

Fig. 3. Discharge capacities of composite electrodes containing porous carbon aerogels with different porosity parameters (rate 70 mA g^{-1}).

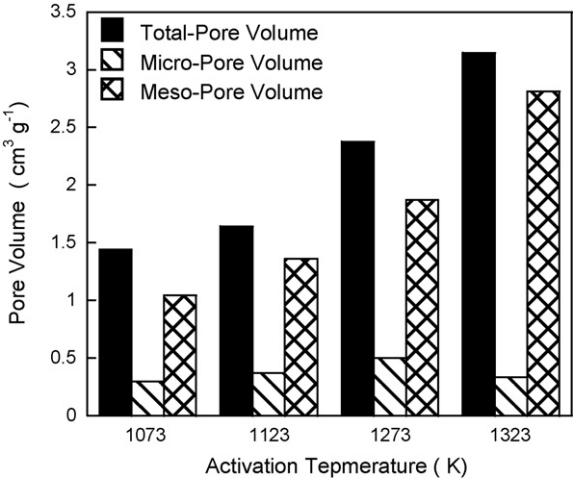

Fig. 4. Total, micro and meso-pore volumes of carbon aerogels activated at various temperatures used in the electrode formulation.

Table 2
Discharge capacities of composite electrodes and carbon aerogels with various pore volumes.

Sample	Cell voltage (V)	Discharge capacity ($mAh\,g^{-1}$)	
		Composite electrode (including MnO_2-related capacity)	Porous carbon (excluding MnO_2-related capacity)
AC-1073 K	2.60	773	243
AC-1123 K	2.64	1206	676
AC-1273 K	2.68	1480	950
AC-1323 K	2.73	1682	1152

It can be seen that the mesopore volume and consequently the total pore volume of carbons increases with increase in the activation temperature. Figs. 3 and 4 show clearly that the storage capacities increase with the development of mesoporosity in carbons. Sample AC-1323 K with the highest mesopore volume showed the highest storage capacity and sample AC-1073 K with the lowest mesopore volume showed the lowest storage capacity between activated carbons.

It is believed that larger pore volume provides more space for the formation and storage of Li_2O_2 during the discharge process as the end-of-discharge of the cell is reached when the pores are filled or choked by the deposition of Li_2O_2 [23].

The role of pore size in air electrode is a key factor affecting the cell performance since appropriate pore size results in better diffusivity of the electrolyte into the carbon structure, better accessibility of lithium ions to the carbon surface and better diffusion of oxygen onto the carbon–electrolyte interface as charge/discharge reaction zone [30].

Fig. 3 and data given in Table 2 also show that the discharge voltage of a Li/O_2 cell depends on the porosity of the carbon used in its cathode electrode. This might be due to the change in the conductivity of carbons with pore size and pore volume [31].

Fig. 5 shows change in the discharge capacity of porous carbon aerogels (as active material in a Li/O_2 cell) with cycle number. It can be seen that the discharge capacity of carbons decreases drastically after 25 cycles. Carbon AC-1323 K shows a significant drop in discharge capacity from 1152 to 147 $mAh\,g^{-1}$ after the 25th cycling. For the rest of carbons shown in Fig. 5 discharge capacities dropped from initial capacities given in Table 2 to below 30 $mAh\,g^{-1}$ after 25th cycling.

In order to study the interfacial changes occurring at the cathode electrode prepared from the aforementioned carbon aerogels with different porous structure and to understand the capacity loss of the cell with charge/discharge cycling, electrochemical impedance spectroscopic analysis (EIS) was conducted.

There are many ways of analyzing EIS data, such as normalization to unit surface area of electrode, or per weight of device. However, since the objective of the paper is the cathode performance focused, EIS results are normalized to unit surface area of electrode disc containing carbons with different porosity parameters, which makes comparisons between EIS results simpler.

The Nyquist plots for cells obtained after the first discharge are shown in Fig. 6.

Fig. 6a shows the EIS pattern of a symmetric "Li/electrolyte/Li" cell measured in Ar atmosphere. This measurement allows understanding of the contribution of anode impedance to the total cell impedance in a Li/O_2 cell. The magnified inset in Fig. 6a shows the EIS spectrum of the symmetric cell clearly.

A comparison between the impedance spectrum in Fig. 6a with the total EIS spectra of Li/O_2 cells shown in Fig. 6b–e confirms the

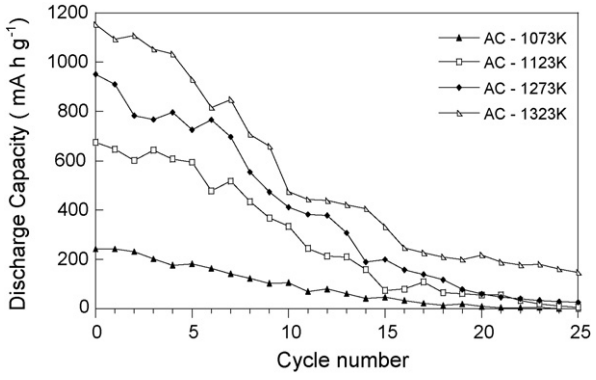

Fig. 5. Variation of discharge capacity of porous carbon aerogels with cycle number.

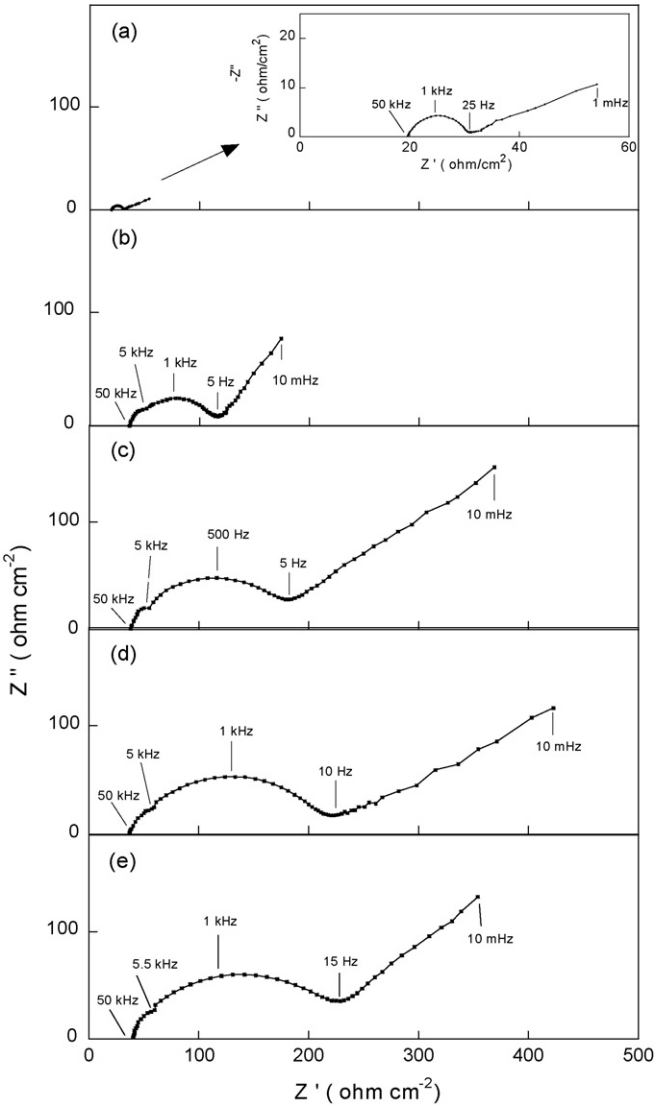

Fig. 6. Impedance spectra of cells after first discharge (rate 70 $mA\,g^{-1}$): (a) symmetric "Li/electrolyte/Li" cell in Ar atmosphere. Li/O_2 cells in O_2 atmosphere containing the following activated carbon aerogels: (b) AC-1073 K, (c) AC-1123 K, (d) AC-1273 K, and (e) AC-1323 K.

weak contribution of the anode to the whole Li/O_2 cell system and shows that the major source of cell impedance in a Li/O_2 cell comes from the cathode [32].

Electrochemical impedance spectra (EIS) of Li/O_2 cells, using four porous carbon aerogels described above are shown in Fig. 6b–e. It can be seen that all impedance spectra in Fig. 6b–e exhibit a high frequency depressed semicircle roughly between 50 and 5 kHz, a medium frequency depressed semicircle in the region of 5 kHz and 10 Hz, and a linear part at the very low frequency side below 10 Hz. This observed behaviour is caused by the dispersion of three different processes with different time constants [33], which are distorted and not well separated. Taking into consideration that the major source of cell impedance comes from the cathode [32], the results of impedance measurements are analyzed as follows.

The high frequency intercept at the real *Z*-axis is corresponded to the electrolyte bulk resistance and electronic resistance of current collector [32,34]. The first relaxation semicircle at high frequencies between 50 and 5 kHz is attributed to the ohmic resistance and film formation involving the combination of electrolyte resistance within the electrode material, reduction of electrolyte species and mainly cathodic deposition and formation of discharge products on the air electrode/electrolyte interface. This also includes the intrinsic electronic resistance of electrode materials and the contact resistance of the carbon particles [32,35]. The semicircle at medium frequency region (5 kHz–10 Hz) is assigned to the parallel combination of the charge-transfer resistance or kinetic resistance related to slow lithium ion transfer coupled with the double layer capacitance of porous cathode [35–37].

The discharge reaction in lithium oxygen batteries is a catalytic reaction between lithium ions (delivered by electrolyte) and oxygen (supplied from the environment through the air electrode) on the porous gas diffusion electrode. Apart from the activity of the catalyst, the electrochemical performance of the battery is dependent on the porosity of the oxygen electrode. The low frequency linear tail with a phase angle of about 45° at very low frequency below 10 Hz shows a dominant mass transport process and indicates the involvement of diffusion control, due to the slow diffusion of electroactive species across the interface between surface films and the catalyst supported carbon along the pores in the air cathode (Warburg effect) [38]; it also involves the capacitive effect of the carbon [32]. It has been argued that the principal transport process of oxygen in a gas diffusion electrode consists of the contributions of: (i) gaseous oxygen diffusion into pores, (ii) oxygen dissolution into the electrolyte film on the catalyst supported electrode, and (iii) dissolved oxygen diffusion across the thin film to the reaction sites [39]. The gaseous diffusion is responsible for impedance at the low frequencies while the ionic diffusion from the bulk of electrolyte to the reaction sites affects impedance mostly at medium frequencies [40].

The shape and values of the resistances in the impedance spectrum is strongly affected by electrode porosity [41]. The diameter of the high frequency semicircles shown in Fig. 6b–e is related to the interfacial resistance between the electrode and electrolyte (R_{int}) which decreases with the pore size probably due to the decreased contact resistance between electrode and electrolyte. The diameter of the medium frequency semicircles is indicative of the charge-transfer resistance (R_{ct}). It can be seen that the charge-transfer resistance also decreases with increasing pore size. This can be attributed to the increased ionic conducting path in the electrode [34,42]. The equivalent circuit in Fig. 7 is used for the quantitative analysis of the EIS spectra [35,43].

In this model the total impedance of the electrode, Z_t, is the sum of electrolyte, interfacial and charge-transfer impedances.

$$Z_t = Z_e + Z_{\text{int}} + Z_{ct}$$

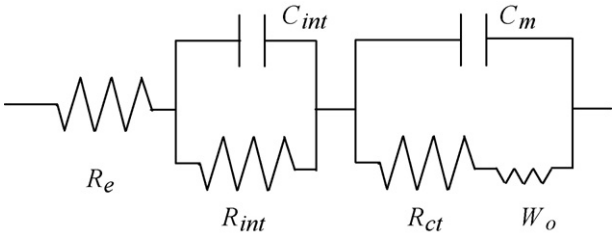

Fig. 7. Equivalent circuit used for the analysis of the impedance plots.

$Z_e = R_e$ is the ionic resistance of electrolyte, Z_{int} is the interfacial impedance indicating the overall ohmic effects and Z_{ct} is the charge-transfer impedance indicating the overall kinetic effects. The equivalent-circuit parameters were obtained by curve fitting using the Zview software (Solartron) with the equivalent circuit shown in Fig. 7.

Fig. 8 shows a typical fitting procedure for the calculation of circuit parameters. In this figure, the calculated and experimental impedance curves for AC-1123 K carbon are compared. As seen, the simulated curve fits entirely with the data measured, indicating that the proposed equivalent circuit represents the cell impedance.

The parameters obtained from the fitting procedure are given in Table 3, where C_{int} is the capacitance of film on the interface between the electrode and electrolyte, C_m is the capacitance for the semicircles at medium frequencies, and W_o is the finite length Warburg (open-circuit terminus) contribution at low frequency behaviour.

The correlation coefficient, which indicates how well the model fits the original data, is above 0.98 for obtaining model parameters given in Table 3. This shows that the estimated parameters are in a good agreement with the experimental data.

Data given in Table 3 shows that electrolyte resistance does not change significantly with change in porous carbon aerogel employed in the oxygen electrode, however there is a significant change in other circuit parameters as the porosity parameters of carbon employed in the oxygen electrode formulation change. Interfacial resistance, R_{int}, increases with increase in the pore volume. This is due to the formation of more discharge products in the structure of oxygen electrode as larger pore volume provide more space for the accommodation of discharge products. The charge-transfer resistance, R_{ct}, is also dependent on the porosity of the carbons significantly. The high values of the charge-transfer resistance are due to the low conductivity of the discharge products [35]. Table 3 shows that the value of R_{ct} increases with increase in the pore volume of the carbon used in the porous electrode, suggesting the amount of discharge products formed within the electrode structure is proportional to R_{ct}, as higher pore volume results in the formation of more discharge products in the cathode structure. The AC-1323 K carbon with the largest total pore and mesopore volumes shows the highest R_{ct}. Yang and Xia [35]

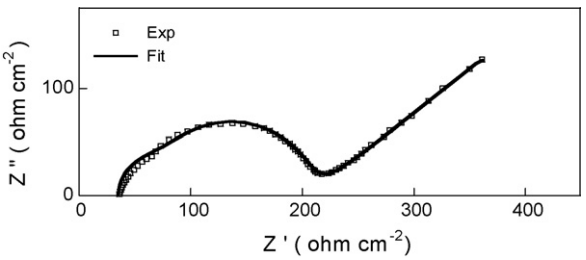

Fig. 8. Measured and calculated impedance spectra of AC-1123 K carbon. Data points are the measured values and the solid line is the calculated impedance curve using the equivalent circuit given in Fig. 7.

Table 3
Dependence of equivalent-circuit parameters upon the porosity of porous carbon aerogels used in the electrode formulation.

Carbon	R_e ($\Omega\,cm^{-2}$)	C_{int} ($F\,cm^{-2}$)	R_{int} ($\Omega\,cm^{-2}$)	C_m ($F\,cm^{-2}$)	R_{ct} ($\Omega\,cm^{-2}$)	W_o ($\Omega\,cm^{-2}$)
AC-1073 K	40.42	1.09×10^{-6}	21.20	37.02×10^{-6}	31.81	0.092
AC-1123 K	39.67	2.91×10^{-6}	31.08	248.13×10^{-6}	53.29	0.165
AC-1273 K	37.43	3.83×10^{-6}	46.82	431.67×10^{-6}	102.03	0.206
AC-1323 K	36.78	10.60×10^{-6}	58.12	508.49×10^{-6}	123.83	0.285

also previously reported that the charge-transfer resistance, R_{ct}, in a Li/O_2 cell increases with an increase in the amount of discharge products formed within the cathode at higher O_2 pressures. The values of R_{ct} for electrodes made of AC-*x* carbons given in Table 3 are consistent with the values of the discharge capacities given in Table 2.

C_{int} and C_m are capacitances, corresponding to R_{int} and R_{ct}, distributed according to the difference in the magnitude of the time constant between ohmic and kinetic processes respectively. The interfacial capacitance, C_{int}, related to the high frequency semicircles leads to the values of the order of $10^{-6}\,F\,cm^{-2}$. This is typical of the capacitance of the oxide surface films as the charge is stored capacitively across the oxide barrier film on the electrode [36]. The value of C_{int} increases with the carbon pore volume and increase in the amount of discharge products formed on the carbon structure.

The capacitance for the semicircles at medium frequencies, C_m, is much higher, compared to the values of C_{int}, that can be ascribed to the high surface area of the porous carbon used in cathode, through which charge transfer occurs [35] combined with pseudocapacitive reaction of MnO_2 used in the composite electrode [44–46]. Considering the simultaneous appearance of double layer capacitance, C_{dl}, attributable to the porous carbon and the pseudocapacitance, C_F, of manganese dioxide in medium frequency region of the impedance spectra, C_m is used to express $C_{dl} + C_F$, though the mechanism between C_{dl} and C_F are different. This capacitance is derived from the fitting procedure explained above and shown in Table 3.

Increase in Warburg resistance, W_o, given in Table 3, is consistent with rationalization of the increase in diffusional resistance with decreasing pore size. The diffusion impedance which appears only for cathodic polarization, increases with decrease in pore size of the carbons used in the electrode formulation, and is probably attributed to the limited diffusion of lithium ions and also gaseous oxygen along the pores.

The impedance spectra of AC-1123 K carbon for cycles following the first cycle are depicted in Fig. 9.

Two consecutive semicircles appeared in the spectra. The high frequency semicircle is related to the cathodic deposition of discharge products on the electrode and electronic resistance of electrode materials. The intercept of this semicircle on the real axis represents the electrolyte bulk resistance and the diameter of the semicircle is related to the interfacial resistance R_{int}. The medium frequency semicircle is assigned to the time constant of charge-transfer resistance and, electrical double layer capacitance and pseudocapacitance on the composite electrode/electrolyte surface. The diameter of the medium frequency semicircle represents the charge-transfer resistance, R_{ct} [37]. This is followed by a slanted line at low frequency range which is characteristic of a diffusion controlled process due to the slow diffusion of lithium ions and also gaseous oxygen within the porous electrode.

The equivalent-circuit parameters were evaluated by the same fitting procedure described above using the equivalent circuit shown in Fig. 7. The calculated parameters are listed in Table 4.

The high frequency semicircles related to the surface films become larger with increasing cycle number [32]. Data given in Table 4 shows that the interfacial resistance, R_{int}, increases from 31.08 to 63.11 $\Omega\,cm^{-2}$ after 20 cycles. This can be explained by the build up of the discharge products within the carbon structure covering a higher portion of the surface with cycling [23,35]. The medium frequency semicircles on the impedance spectra shows that the charge-transfer resistance is quite large compared with the ohmic resistance and increases significantly from 53 to 440 $\Omega\,cm^{-2}$ after 20 cycles. Extremely high charge-transfer resistance is ascribed to the low conductivity of the discharge products [35] and increase in R_{ct} with cycle number is due to the pore filling and accumulation of low conductive products on the surface impeding lithium ion transfer and charge transfer within the carbon structure.

The corresponding capacitances C_{int} and C_m obtained from fitting procedure are in the order of $10^{-6}\,F\,cm^{-2}$ for the high

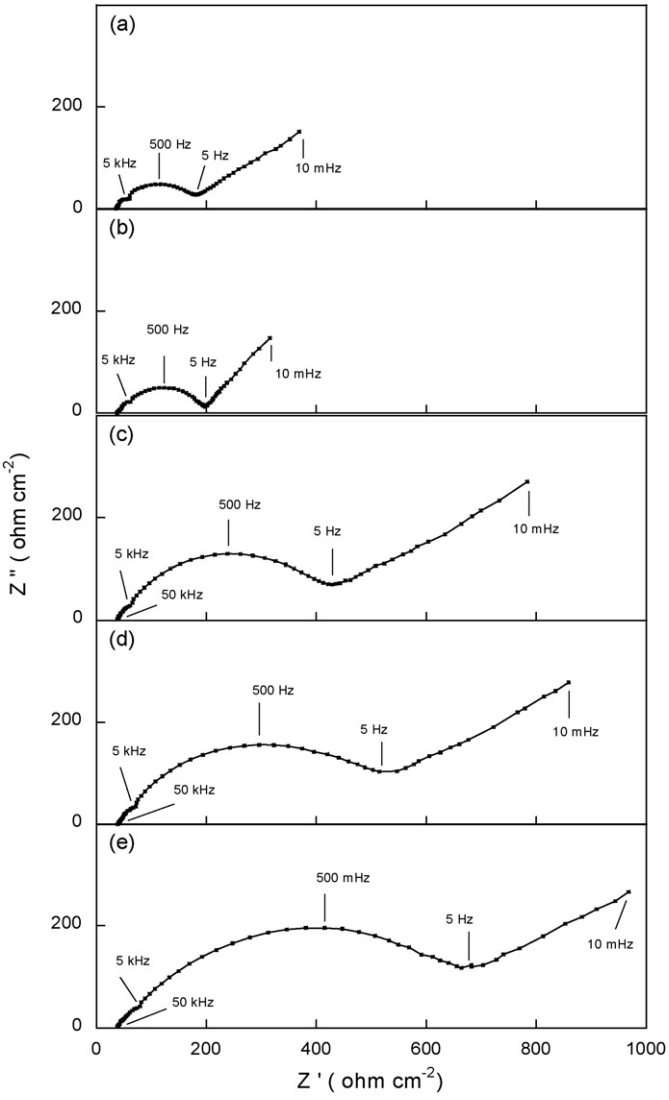

Fig. 9. EIS spectra of AC-1123 K carbon with cycling tests at a discharge rate of 70 mA g^{-1}: (a) after 1st cycle, (b) after 5th cycle, (c) after 10th cycle, (d) after 15th cycle, and (e) after 20th cycle.

Table 4
Equivalent-circuit parameters of AC-1123 K carbon for different cycles.

Cycle	R_e ($\Omega\,cm^{-2}$)	C_{int} ($F\,cm^{-2}$)	R_{int} ($\Omega\,cm^{-2}$)	C_m ($F\,cm^{-2}$)	R_{ct} ($\Omega\,cm^{-2}$)	W_o ($\Omega\,cm^{-2}$)	Ability to deliver a specific performance compared to the fresh cell (%)
1st	39.67	2.91×10^{-6}	31.08	248.13×10^{-6}	53.29	0.165	100 (fresh cell)
5th	38.36	2.43×10^{-6}	34.21	377.62×10^{-6}	68.66	0.184	74.3
10th	39.16	2.35×10^{-6}	53.40	238.17×10^{-6}	299.37	0.226	53.8
15th	39.22	1.78×10^{-6}	56.27	189.75×10^{-6}	340.62	0.255	32.7
20th	40.03	1.39×10^{-6}	63.11	106.46×10^{-6}	440.80	0.308	23.2

frequency semicircles, and $10^{-4}\,F\,cm^{-2}$ for medium frequency semicircles respectively. The low value of C_{int} is typical of surface films formed on the electrode [47].

C_m represents the double layer capacitance, C_{dl}, associated with the electroactive surface area of the porous carbon [48] coupled with pseudocapacitance, C_F, attributable to manganese dioxide, in the composite cathode electrode [35,44–46]. Decrease in the C_m values with concomitant increase in the resistance terms shown in Table 4, indicates that a higher portion of the electrode's surface gets covered by the discharge products with increasing cycle number.

The impedance data in Table 4 shows that the internal resistance of the cell increases with repeating charge and discharge. This indicates that charge/discharge cycling causes significant interfacial changes in the air electrode hindering the passage of lithium ions to the electrode surface where oxygen is reduced catalytically, and subsequently impeding the discharge reaction. It is believed that as the cell discharges cyclically, Li_2O_2 built up in the pores results in change in the porosity of the cathode electrode obstructing the transfer of oxygen and lithium ions to the reaction sites. Formation of the discharge products and exposure of the electroactive surface area to low conductive discharge products by cycling also decreases the electrolyte accessible surface of the electrode resulting in significant decrease in C_m.

To describe change in the performance of porous carbon as active material in the cathode electrode of a Li/O_2 cell with cycling, the performance of the cell using AC-1123 K carbon as active material for different cycles is compared and given in Table 4. The capacity of the fresh cell obtained at the end of the first discharge is corresponded to a performance of 100%. Performance of the cell at cycles after the first cycle given in Table 4, reflects the ability of the porous carbon with cycling to deliver the specific capacity compared to that of the fresh cell. As we can see the performance of the cell decreases with charge discharge cycling and deteriorates to 23.2% of the specific performance of the fresh cell after 25 cycles. This indicates that the cell starts to fail in storing and delivering electric energy presumably once the carbon pores are getting filled with the build up of discharge products and oxygen is unable to reach the carbon–electrolyte interface active sites for the net cathodic electrochemical reaction to occur due to pore plugging with the solid product. This results in significant decrease in the cell capacity and deterioration of the cell performance during its life time due to the irreversible physical and chemical changes that take place at the cathode air electrode.

Change in the discharge capacity with cycle number for AC-1123 K carbon in Fig. 5 shows that the rate of degradation of the cell increases sharply after the first five cycles. Data given in Table 4 also shows a sudden increase in the values of R_{int}, R_{ct} and W_o after the first five cycles for this carbon. Increase in the cell impedance with cycle number, shown in Table 4, results in a significant decrease in the storage capacity of the cell after 25 cycles. This shows that large surface resistance to electron or ion transfer will result in slow kinetics, large activation polarizations and leads to a significant loss of cycling efficiency and capacity fading. In fact the presence of resistive layers formed on the cathode surface may result in the reduction of ion transfer within the electrode to levels where their concentration can no longer support the current demand. The lack of electron transfer must be compensated by removing some electrons from other species in the cell (i.e. electrolyte) irreversibly, leading to capacity fading and loss of cycling efficiency [41].

Pores in carbon electrode allow both the reduced oxygen ions and electrolyte containing lithium ions, to come in contact. The electrochemical reduction of oxygen takes place on the carbon surface. It is important to minimize diffusion barriers, and ionic and electronic resistances to decrease the internal resistance, improve storage capacity, and stabilize discharge capacity and potential of Li/O_2 cells. These can be achieved by engineering carbons having appropriate porous structure and pore size that facilitates electrolyte and oxygen accessibility to the porous network of the air electrode.

Although major part of the cell impedance comes from the cathode electrode, however the relaxation loop related to the impedance of passivated film can also be affected by the anode and its initial state. The lower the oxidation of the lithium metal surface used in a fresh cell at the beginning, the smaller the passivated film impedance on the anode surface [32].

Increase in the finite length Warburg resistance (open-circuit terminus), W_o, with cycle number shown in Table 4 shows a gradual increase in the diffusion impedance resulting from the slow diffusion of electroactive species along the pores within the air cathode. The most probable reason for this is change in the porosity of the electrode with cycling which results in a decrease in the oxygen and lithium ion diffusion due to the build up of discharge products within the pores.

4. Conclusions

Air cathode electrodes based on RF carbon aerogels with controlled porous structure at nano-scale were prepared and their electrochemical performance in a lithium oxygen cell was evaluated by galvanostatic charge/discharge and electrochemical impedance spectroscopy measurements. To our knowledge this work is the first to demonstrate the use of electrochemical impedance spectroscopy as a powerful technique for studying the capacity loss due to the interfacial changes occurring at the air cathode of a lithium oxygen battery.

Galvanostatic charge/discharge measurements showed that the storage capacity of a lithium oxygen battery increases with the mesoporosity of carbon used in the cathode, suggesting mesoporosity in carbon is a key factor affecting the lithium oxygen cell performance. A Li/O_2 battery using the carbon with pore volume of $3.146\,cm^3\,g^{-1}$ and average pore diameter of 17.37 nm showed a specific capacity of $1682\,mAh\,g^{-1}$ and discharge voltage of 2.73 V.

EIS results demonstrate that the shape and value of the resistance in the impedance spectrum of a Li/O_2 cell is strongly affected by the porosity of the carbon employed in cathode electrode. This shows that a qualitative improvement in lowering the impedance response of the lithium oxygen cell can be achieved by tailoring the porous structure of the carbon used in the air cathode electrode.

Gradual build up of discharge products in the pores of the carbon with cycling, changes the porosity of the electrode and therefore the ability of oxygen and lithium ions to diffuse into the electrode

structure, leading to a significant increase in the cell impedance. This will result in slow kinetics and large activation polarizations, and terminates to the capacity fading and loss of cycling efficiency. The results obtained from this study showed that cycle life of a lithium oxygen cell decreases as its internal resistance increases with repeat of charge and discharge. Therefore it is important to minimize diffusion barriers, and ionic and electronic resistances to decrease the internal resistance by engineering carbon electrodes having appropriate porous structure and pore size that facilitate electrolyte and oxygen accessibility to the porous network of the air cathode electrode.

Acknowledgment

This work was funded by the EPSRC as part of the Supergen Energy Storage Consortium (Grant code EP/D031672/1).

References

[1] Survey of Energy Resources – Executive Summary, Published by World Energy Council, London, 2007.
[2] D. Linden, T.B. Reddy, Battery Power Magazine 12 (2) (2008) 10–13.
[3] J.-M. Tarascon, M. Armand, Nature 414 (2001) 359–367.
[4] C.S. Johnson, J. Power Sources 165 (2007) 559–565.
[5] P. Poizot, S. Laruelle, S. Grugeon, L. Dupont, J.-M. Tarascon, Nature 407 (2000) 496–499.
[6] S. Patoux, M. Dolle, M.M. Doeff, Chem. Mater. 17 (2005) 1044–1054.
[7] Y. Hu, W. Kong, Z. Wang, X. Huang, L. Chen, Solid State Ionics 176 (2005) 53–56.
[8] B. Xie, H.S. Lee, H. Li, X.Q. Yang, J. McBreen, L.Q. Chen, Electrochem. Commun. 10 (2008) 1195–1197.
[9] K. Xu, M.S. Ding, S. Zhang, J.L. Allen, T.R. Jow, J. Electrochem. Soc. 149 (2002) A622–A626.
[10] F.F.C. Bazito, R.M. Torresi, J. Braz. Chem. Soc. 17 (2006) 627–642.
[11] H.D. Abruna, Y. Kiya, J.C. Henderson, Phys. Today 61 (12) (2008) 43–47.
[12] A. Debart, J. Bao, G. Armstrong, P.G. Bruce, J. Power Sources 9 (2007) 1177–1182.
[13] S. Zaromb, J. Electrochem. Soc. 109 (1962) 1125–1129.
[14] D. Linden, B.T. Reddy, Handbook of Batteries, 3rd ed., McGraw-Hill, New York, 1989.
[15] G.Q. Zhang, X.G. Zhang, Y.G. Wang, Carbon 42 (2004) 3097–3102.
[16] W. Li, C. Li, C. Zhou, H. Ma, J. Chen, Angew. Chem. 118 (2006) 6155–6158.
[17] G.G. Kumar, N. Munichandraiah, Electrochim. Acta 44 (1999) 2663–2666.
[18] A. Patrick, M. Glasse, R. Latham, R. Linford, Solid State Ionics 18–19 (1986) 1063–1067.
[19] J.J. Xu, H. Ye, Electrochem. Commun. 7 (2005) 829–835.
[20] K.M. Abraham, Z. Jiang, J. Electrochem. Soc. 143 (1996) 1–5.
[21] T. Ogasawara, A. Debart, M. Holzapfel, P. Novak, P.G. Bruce, J. Am. Chem. Soc. 128 (2006) 1390–1393.
[22] J. Read, J. Electrochem. Soc. 149 (2002) A1190–A1195.
[23] M. Mirzaeian, P.J. Hall, J. Power Syst. Technol. 31 (2007) 90–97.
[24] M. Mirzaeian, P.J. Hall, J. Mater. Sci. 44 (2009) 2705–2713.
[25] S.J. Gregg, K.S.W. Sing, Adsorption, Surface Area and Porosity, Academic Press, New York, 1967.
[26] M. Kuk, M. Jaroniec, K.P. Gadkaree, J. Colloid Interface Sci. 192 (1997) 250–256.
[27] D. Mowla, D.D. Do, K. Kaneko, in: L.R. Radovic (Ed.), Chemistry and Physics of Carbon, vol. 28, Marcel Dekker, New York, 2003, pp. 229–262.
[28] Y. Yan, J. Wei, F. Zhang, Y. Meng, B. Tu, D. Zhao, Micropor. Mesopor. Mater. 113 (2008) 305.
[29] M.M. Thackeray, M.H. Rossouw, A. de Kock, A.P. de la Harpe, R.J. Gummow, K. Pearce, D.C. Liles, J. Power Sources 43–44 (1993) 289–300.
[30] M. Mirzaeian, P.J. Hall, Electrochim. Acta 54 (2009) 7444–7451.
[31] V.F. Surovikin, A.G. Shaitanov, N.N. Leot'eva, V.A. Drozdov, Solid Fuel Chem. 5 (2009) 318–327.
[32] J.Y. Song, H.H. Lee, Y.Y. Wang, C.C. Wan, J. Power Sources 111 (2002) 255–267.
[33] N. Takami, A. Satoh, M. Hara, T. Ohsaki, J. Electrochem. Soc. 142 (1995) 371–379.
[34] H. Wang, H. Huang, S.L. Wunderz, J. Electrochem. Soc. 147 (2000) 2853–2861.
[35] X. Yang, Y. Xia, J. Solid State Electrochem. 14 (2010) 109–114.
[36] M.D. Levi, G. Salitra, B. Markovsky, H. Teller, D. Aurbach, U. Heider, L. Heiderb, J. Electrochem. Soc. 146 (1999) 1279–1289.
[37] H.S. Kim, C.W. Lee, S.I. Moon, J. New Mater. Electrochem. Syst. 9 (2006) 15–20.
[38] F. Croce, F. Nobili, A. Deptula, W. Lada, R. Tossici, A. D'Epifanio, B. Scrosati, R. Marassi, Electrochem. Commun. 1 (1999) 605–608.
[39] D.B. Zhou, H. Vander Poorten, Electrochim. Acta 40 (1995) 1819–1826.
[40] H. Arai, S. Müller, O. Haas, J. Electrochem. Soc. 147 (2000) 3584–3591.
[41] J.B. Kerr, in: G. Nazri, G. Pistoia (Eds.), Lithium Batteries: Science and Technology, Kluwer Academic Publishers, Norwell, 2004, (Chapter 19).
[42] S. Ahn, B.J. Tatarchuk, J. Electrochem. Soc. 142 (1995) 4169–4175.
[43] T. Tonosaki, T. Oho, K. Isomura, K. Ogura, J. Electroanal. Chem. 520 (2002) 89–93.
[44] K.W. Leitner, B. Gollas, M. Winter, J.O. Besenhard, Electrochim. Acta 50 (2004) 199–204.
[45] X. Dong, W. Shen, J. Gu, Li. Xiong, Y. Zhu, H. Li, J. Shi, J. Phys. Chem. B 110 (2006) 6015–6019.
[46] H. Adelkhani, J. Electrochem. Soc. 156 (2009) A791–A795.
[47] J.S. Gnanaraj, M.D. Levi, E. Levi, G. Salitra, D. Aurbach, J.E. Fischer, A. Claye, J. Electrochem. Soc. 148 (2001) A525–A536.
[48] F. Alcaide, E. Brillas, P.-L. Cabot, J. Electrochem. Soc. 150 (2003) E52–E58.